RESEARCH ARTICLE

Editor's Choice

ADVANCED MATERIALS INTERFACES Open Access

www.advmatinterfaces.de

Antifouling Surface-Attached Hydrogel Nanocoatings Redefined: Green Solvent-Based, Degradable, and High-Performance Protection Against Foulants

Jenny Englert, Marc Palà, Jonas Quandt, Hannah Sieben, Oliver Grottke, Bernd Marx, Gerard Lligadas, and Cesar Rodriguez-Emmenegger**

Antifouling coatings are vital to enhance the performance of medical devices, aiming to mitigate bodily reactions by shielding their surface. Despite significant advancements in antifouling coatings, like those based on zwitterionic monomers and hydroxyl-functionalized (meth)acrylamides, limitations like decreased antifouling properties after functionalization and complement system activation hinder their application in blood. Here, a novel class of ultrathin surface-attached hydrogels is presented, consisting of hydrophilic non-charged green solvent-based monomers and preventing protein adsorption while offering on-demand degradability. Unlike the best antifouling brushes, the coatings are easily applicable, unaffected by charges, and free of complement system-activating groups. The hydrogels are formed using copolymers of *N*,*N*-dimethyl lactamide acrylate (DMLA) and benzophenone acrylate (BPA). Moreover, 5,6-benzo-2-methylene-1,3-dioxepane (BMDO) is incorporated to introduce hydrolyzable ester. The coating of state-of-the-art devices is demonstrated with X-ray photoelectron spectroscopy (XPS), analyze surface energy components, and confirm their antifouling properties with surface plasmon resonance (SPR). The coatings are non-cytotoxic toward MRC-5 fibroblasts, exhibit repellency against methicillin-resistant *Staphylococcus aureus* (MRSA), and effectively prevent thrombus formation on devices in blood. This work establishes a versatile platform for next-generation coatings in medical and industrial applications, matching the antifouling efficiency of the most advanced solutions and offering regeneration of substrates by erasing the coating.

1. Introduction

Fouling presents a significant challenge, particularly in the biomedical field. The interface between medical devices and bodily fluids frequently becomes a hotspot for protein adsorption, which can initiate inflammatory responses, macrophage recruitment, granulation tissue formation, and bacterial colonization.[1–4] This is further aggravated when blood is the contacting fluid, because it inevitably leads to the activation of coagulation, exciding the self-regulatory action of hemostasis and leading to clot formation on the surface, which affects the performance of the device.[1,3,5] In recent decades, significant strides have been made to develop antifouling coatings that restrict the non-specific adsorption of proteins, cells, bacteria, and other biological components, thereby enhancing the biocompatibility of medical devices. Among these advancements, hydrophilic polymer brushes have emerged as the most successful antifouling coatings, with poly(ethylene glycol) (PEG)-based brushes being the most prominent.[6–10]

J. Englert, J. Quandt, C. Rodriguez-Emmenegger
DWI – Leibniz Institute for Interactive Materials
Forckenbeckstraße 50, 52074 Aachen, Germany
E-mail: rodriguez@dwi.rwth-achen.de

M. Palà, G. Lligadas
Universitat Rovira i Virgili
Departament de Química Analítica i Química Orgànica
Laboratory of Sustainable Polymers
Tarragona 43007, Spain
E-mail: gerard.lligadas@urv.cat

The ORCID identification number(s) for the author(s) of this article can be found under https://doi.org/10.1002/admi.202500122

DOI: 10.1002/admi.202500122

H. Sieben, O. Grottke
Department of Anesthesiology
RWTH Aachen University Hospital
52074 Aachen, Germany

B. Marx
Vygon GmbH & Co. KG – Medizintechnik
Prager Ring 100, 52070 Aachen, Germany

C. Rodriguez-Emmenegger
Institute for Bioengineering of Catalonia (IBEC)
The Barcelona Institute of Science and Technology (BIST)
Carrer de Baldiri Reixac 10–12, Barcelona 08028, Spain

C. Rodriguez-Emmenegger
Institució Catalana de Recerca i Estudis Avançats (ICREA)
Passeig Lluís Companys 23, Barcelona 08010, Spain

However, despite their extensive study, PEG-based brushes exhibit not robust antifouling performance with high donor variability.[11] PEG-based brushes have been shown to adsorb at least nine different proteins from human blood plasma.[12–14] Furthermore, PEG-based coatings were shown to be able to activate the complement system in blood which was attributed to the presence of hydroxyl groups, making it less suitable for use in blood-contacting medical devices.[12,13] More advanced antifouling coatings base on zwitterionic monomers like phosphorylcholines,[15–17] sulfobetaines,[8,18–21] and carboxybetaines.[8,18,20,22] Among these, carboxybetaines exhibit superior antifouling properties even in undiluted human blood plasma—one of the most challenging bodily fluids—and can also be functionalized.[8] Another class of antifouling polymer brushes are made of hydroxyl-functionalized (meth)acrylamides, which have demonstrated outstanding repulsion against proteins, cells, and bacteria.[23–31] Despite the advancements of these coatings, research has revealed that the antifouling properties of carboxybetaine-based coatings decrease after functionalization, likely due to alterations in their net charge.[32,33] Moreover, the hydroxyl-functionalized (meth)acrylates and (meth)acrylamides, coatings have been reported to activate the complement system in blood, restricting their suitability for blood-contacting medical devices.[12,34,35] Incipient work antifouling coatings of poly(oxazoline) suggests that there might be alternatives to zwitterionic and hydroxyl-functional (meth)acrylamides to achieve antifouling properties.[36]

In this work, we introduce a new type of surface coating that is based on easily applicable ultrathin surface-attached hydrogels that prevents non-specific protein adsorption and can be degraded on demand. We applied them on various commercially available state-of-the-art medical devices and confirmed their successful repulsion of bacteria and full human blood.

The coatings root on the concept of ultrathin surface-attached hydrogels where hydrophilic polymer chains connect via crosslinking points while being anchored to the surface.[37–41] These coatings can only swell orthogonally to the surface and were shown to possess a brush-like interface due to the migration of polymer chains to the interface.[40] Here, we synthesized ultrathin surface-attached hydrogels using a terpolymer of DMLA, BPA, and BMDO (**Figure 1**). DMLA, a monomer derived from lactic acid using the green biosolvent *N*,*N*-dimethyl lactamide, was shown to display excellent antifouling properties in brushes.[34] It is strongly hydrophilic, while unlike zwitterionic monomers, it is largely unaffected by ionic interactions.[34,42–44] Moreover, it avoids complement system activation in blood, as it lacks hydroxyl groups.[34] BPA contains benzophenone units needed for the crosslinking of the polymer chains and formation of the coating.[37–40] Upon UV irradiation, the benzophenone units perform a C,H-insertion with neighboring polymeric chains and with C-H bonds present on the surface, simultaneously generating the covalently linked hydrogel, as well as covalently attaching the hydrogel to the surface. The integration of BMDO introduces ester bonds along the polymer fragments which can be cleaved in acidic and alkaline conditions. The polymers were prepared by radical polymerization of DMLA, BPA, and BMDO (radical ring-opening polymerization, rROP) and characterized by ^{1}H nuclear magnetic resonance (NMR) spectroscopy and size exclusion chromatography (SEC). BMDO was distributed homogeneously along the polymer chain, which enables degradation into homogenous oligomeric fractions and lactic acid, a metabolite, yielding complete disassembly of the nanoscale coating. This feature offers advantages such as the potential for fully erasing the coating.

We synthesized polymers with and without BPA, while those with BPA were applied onto model substrates (modified flat silicon), poly(ε-caprolactone) (PCL) meshes, hernia meshes, central venous catheters (CVCs) which are widely utilized in clinics, and flat poly(4-methyl-1-pentene) (PMP) as utilized for extracorporeal membrane oxygenators (ECMO). The coating formation was confirmed with XPS and ellipsometry. Moreover, we assessed their degradation behavior in solution and on the surface. All coatings resulted in outstanding repellency against proteins, a clinical strain of MRSA, and even against full human blood. This work showcases the ability to achieve exceptional antifouling performance using a novel hydrophilic monomer that surpasses the efficacy of leading antifouling monomers, such as zwitterionic or hydroxyl-functionalized (meth)acrylamides, while also being degradable on demand. We envision our coatings to strongly contribute to future applications in various scientific and industrial fields.

2. Results and Discussion

2.1. Polymer Synthesis and Characterization

The monomers, BMDO, DMLA, and BPA were synthesized according to previously published procedures[34,40,42,43,45,46] (Supporting Information). They polymerized by reversible addition-fragmentation chain-transfer (RAFT) polymerization in anhydrous DMSO, where BMDO was integrated along the backbone by rROP mechanism.[47] A M/CTA of 200 is equal to a maximal degree of polymerization at full conversion, while varying the DMLA/BMDO ratio at feed between 0 and 0.4 (**Table 1**, entries 1–5). The content of BMDO in the polymer was calculated analyzing ^{1}H-NMR, by integrating overlapped proton *p* (–C*H*–) from DMLA and proton *j* (–OCH_2–) from BMDO, respectively, at 5.5–5 ppm (Figures S2 and S3, and ES1–S3, Supporting Information). BMDO incorporation into the main chain ranged from contents of 0–0.24, being approximately half of the ratio of its feed. Negligible BMDO incorporation was observed for $f_{BMDO} < 0.2$, which is likely due to lower reactivity compared to acrylic monomers.[48] Incorporation of unopened BMDO was depreciable since no significant signal was observed in the range of 4.8–4.5 ppm, associated to –OCH_2– protons from closed monomer.[49] Increasing of the feed of BMDO (f_{BMDO}) resulted in a decreasing of DMLA conversion (from 100% to 75%) after 16 h of reaction time, which may be attributed to the lower reactivity of BMDO. The molecular

C. Rodriguez-Emmenegger
Biomedical Research Networking Center in Bioengineering Biomaterials and Nanomedicine
The Institute of Health Carlos III
Madrid 28029, Spain

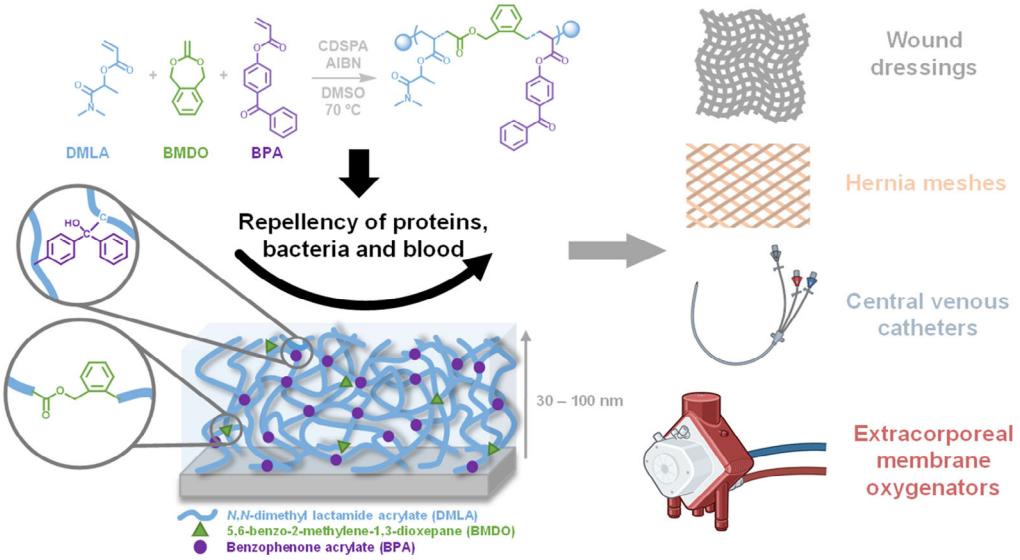

Figure 1. Concept of the degradable green solvent-based ultrathin surface-attached hydrogel coatings. DMLA is copolymerized with a BPA and BMDO, allowing the generation of a hydrolytically degradable surface-attached hydrogel upon irradiation (Figure S1, Supporting Information). This versatile coating can be applied on different medical substrates, rendering them stealth in the body to prevent surface-associated complications. Created with BioRender.

weights were determined with size exclusion chromatography (SEC) and ranged between 11 400 and 19 600 g·mol^{-1}. All polymers displayed monomodal SEC elugrams (Figure S4, Supporting Information). The polydispersity was lowest for the homopolymer p(D) ($Đ$ = 1.45) and monotonically increased with the BMDO content until $Đ$ = 1.75. This may be caused by the lower rate of propagation. BPA was introduced into the polymers as a crosslinker to enable the formation of the ultrathin surface-attached hydrogels (Table 1, entries 6–9). Copolymerization of DMLA and BPA for 2 h yielded copolymers with high DMLA conversions, molecular weights ≈20 000 g·mol^{-1}, and narrow dispersity ($Đ$ < 1.45), attributable to the similar propagation rate of the methacrylic DMLA and BPA. Terpolymer compositions were analyzed by ^{1}H-NMR after dialysis (Figure S5 and ES4–ES6, Supporting Information) and revealed similar DMLA conversions, molecular weights, and dispersity as for the copolymers.

We examined the solubility behavior of DMLA copolymers with different ratios of hydrophobic BMDO and BPA (Figure S6, Supporting Information). Phase transition temperatures (T_{cp}) of the polymers were determined by optical transmission measurements of their aqueous solutions prepared at 10 mg·mL^{-1}. The T_{cp} decreased linearly from 53.4 °C to 24.2 °C and from 71 °C to 46.1 °C upon increasing BMDO and BPA content respectively in the copolymer with DMLA due to the hydrophobic nature of BMDO and BPA. The same trend was observed when increasing the content of the hydrophobic monomers in the terpolymers, which led to a reduction of T_{cp} from 59.2 °C with 6% of hydrophobic monomers to 30.9 °C with 20% of hydrophobic monomers in a reversible manner.

Table 1. RAFT polymerization of DMLA, BMDO, and BPA-containing copolymers.

Entry	Reference	f_{BMDO}	F_{BMDO} [a]	F_{BPA} [a]	DMLA conv. (%) [b]	$M_n^{(NMR)}$ [a]	$M_n^{(SEC)}$ [c]	$Đ$ [c]	T_{cp} (°C) [d]
1	p(D)	–	–	–	100 [e]	17 900	19 600	1.45	Soluble
2	p($D_{91\%}$-$BM_{9\%}$)	0.25	0.09	–	96	19 900	15 900	1.70	53.4
3	p($D_{84\%}$-$BM_{16\%}$)	0.30	0.16	–	88	19 400	14 300	1.65	43.2
4	p($D_{81\%}$-$BM_{19\%}$)	0.35	0.19	–	75	14 500	11 400	1.68	32.9
5	p($D_{76\%}$-$BM_{24\%}$)	0.40	0.24	–	83	21 400	12 100	1.75	24.2
6	p($D_{99\%}$-$BP_{1\%}$)	–	–	0.01	95 [e]	18 800	18 700	1.45	71 [f]
7	p($D_{95\%}$-$BP_{5\%}$)	–	–	0.05	94 [e]	16 700	27 700	1.29	46.1
8	p($D_{94\%}$-$BM_{5\%}$-$BP_{1\%}$)	0.22	0.05	0.01	100	16 600	18 900	1.65	59.2
9	p($D_{80\%}$-$BM_{14\%}$-$BP_{6\%}$)	0.28	0.14	0.06	94	19 000	18 800	1.85	30.9

f: molar ratio of BMDO at t = 0 and no conversion. It is calculated as the ratio of the moles of BMDO to the sum of the moles of all monomers. *F*: fraction of monomer in the polymer. [a] Determined by ^{1}H NMR (ES1–S6, Supporting Information); [b] Determined by ^{1}H NMR after 16 h of reaction time; [c] Determined by SEC using PMMA standards; [d] Determined by UV/Vis spectroscopy (c = 10 mg·mL^{-1}, heating rate = 0.5 °C·min^{-1}); [e] Reaction time: 2 h; [f] Determined visually (c = 10 mg·mL^{-1}).

Table 2. Static contact angles, surface energy components, hydrophobicity, and Chen Qi ratio of the ultrathin surface-attached hydrogels on modified silicon.

	Static contact angle [°]			Surface energy components [mJ·m^{-2}]				Hydrophobicity [mJ·m^{-2}]	Chen Qi ratio
	θ_W	θ_F	θ_B	γ^{LW}	γ^+	γ^-	γ^{AB}	ΔG^H	
1	33 ± 4	30 ± 4	25 ± 3	41.2	0.4	45	8.4	23	0.9
2	34 ± 1	29 ± 3	30 ± 2	39.5	0.7	43	10.9	20	0.9
3	41 ± 2	34 ± 2	16 ± 3	43.6	0.2	38	5.0	13	1.1

1: p($D_{99\%}$-$BP_{1\%}$), 2: p($D_{94\%}$-$BM_{5\%}$-$BP_{1\%}$), 3: p($D_{80\%}$-$BM_{14\%}$-$BP_{6\%}$), static water contact angles in water (θ_W), formamide (θ_F), and α-bromonaphthalene (θ_B), γ^+: Lewis acid parameter, γ^-: Lewis base parameter, γ^{AB}: Lewis acid-base component.

Such behavior has been observed previously with other DMLA copolymers.[44,50]

2.2. Formation and Characterization of Surface-Attached Hydrogels

The ultrathin surface-attached hydrogels were formed by spin-coating or deposition of a solution of BPA-containing polymers (10 mg·mL^{-1} in water) onto the substrates, followed by irradiation with UV light for 30 min. The concept of surface-attached hydrogels has been explored by Rühe,[37–39,51–55] Prucker,[38,51–55] others,[56–59] and our group.[40,41] The mechanism is based on the deposition of a polymer that contains a small proportion of a monomer, that upon external trigger can perform a C,H-insertion with neighboring polymer chains and the substrate. Such monomers include (sulfonyl) azides, diaziridines, diazocarbonyls, and aromatic carbonyls like benzophenone.[38,39] In our polymers we implement 1–6% of BPA, which contains benzophenone units. In particular for benzophenone, the mechanism is based on the homolytic cleavage of the carbonyl bond of the benzophenone, which is triggered by UV irradiation and leads a biradical triplet state (Figure S1, Supporting Information).[39] The oxygen radical abstracts a hydrogen from a C-H group of either neighboring polymer chains or from the surface, resulting in the formation of a hydroxyl group. This causes the formation of a radical at the carbon atom from the previous C-H group. The carbon radicals from the carbonyl bond and the previous C-H bond can then recombine to form a stable covalent bond. This means that the formation of the hydrogel happens simultaneously with the linking to the surface. The only prerequisites for successful hydrogel adherence are the presence of C-H bonds on the surface and adequate coverage of the surface with the polymer solution to ensure uniform coating. The formation of the hydrogel coating can be carried out by deposition of the polymer, followed by drying and UV irradiation, or by irradiating a material that is placed in the polymeric solution. The latter is especially useful for materials with complex structures. This allowed us to not only coat meshes and electrospun fibers, but also human hair and the fibers of ECMOs. In this way, longer irradiation times lead to thicker coatings. The coating of PCL meshes, hernia meshes, CVCs and flat PMP was confirmed with XPS (Figures S7–S10 and Tables S1 and S2, Supporting Information). The coating thickness was determined by ellipsometry and adjusted to ≈10–20 nm for XPS measurements, analysis of the components of the surface energy, and analysis of bacteria adhesion and hemocompatibility (Table S3, Supporting Information).

Protein fouling has been associated with the strength of collective weak interactions such as Coulombic,[60–62] dipole-dipole, van der Waals, and hydrophobic effect which can be collectively considered as the using the surface energy. The components of the surface energy, the Lewis base parameter (γ^-), Lewis acid parameter (γ^+) and the hydrophobicity, defined as the Gibbs free energy between two surfaces in water (ΔG^H) were determined with a thermodynamic analysis based on the van Oss acid-base approach as previously described (**Table 2** and Equations S7–S10, Supporting Information).[34,40,46,63] For that, we determined the static contact angles (θ) of the coatings on silicon substrates in two polar (water and formamide) and a nonpolar (α-bromonaphthalene) liquid via the captive bubble method. All coatings displayed water contact angles considerably lower than 90° owing to their high wettability. The water contact angles of the ultrathin surface-attached hydrogels were similar to those of poly(DMLA) brushes.[34] Furthermore, increasing the BMDO content led to marginally increased water contact angles, likely attributable to its hydrophobic nature. Besides that, the positive values of ΔG^H underline the hydrophilic properties of the coatings, with the polymers low in BMDO content being more hydrophilic. Moreover, γ^- exceeded γ^+ in all coatings, which indicates a surplus of electron donors. Also, we calculated the Chen Qi ratio (γ^{LW}/γ^-) which gives indication about the adhesion of bacteria to surfaces, with lower values hinting less adhesion.[64,65] All coatings displayed similarly low Chen Qi ratios, suggesting strong repellency against bacteria. Notably, the Chen Qi ratios of the ultrathin surface-attached hydrogels were close to those determined for poly(DMLA) brushes.[34] The thermodynamic analysis proves the strong hydrophilic properties of the coatings, which suggests a high interaction with water.

2.3. Degradation Behavior in Solution and on the Surface

We assessed the hydrolytic degradation of the prepared polymers in solution at pH 1 and 13, as well as in a range of milder pH and PBS buffer. At pH 13, ^{1}H NMR revealed the transformation of p(D) into poly(acrylic acid) and DML by the complete cleavage of the ester side groups after 24 h. DMLA was further hydrolyzed to lactic acid, a green product (Figure S11, Supporting Information).[44] The other extreme condition, pH 1, resulted in negligible degradation after 1 d, whereas after 7 days the NMR spectrum showed degradation accompanied by a reduction of the M_n from 19600 to 6600 g·mol^{-1} as obtained by SEC (**Figure 2A**; Figure S11, Supporting Information). If every side chain of DMLA is hydrolyzed, the expected M_n for the

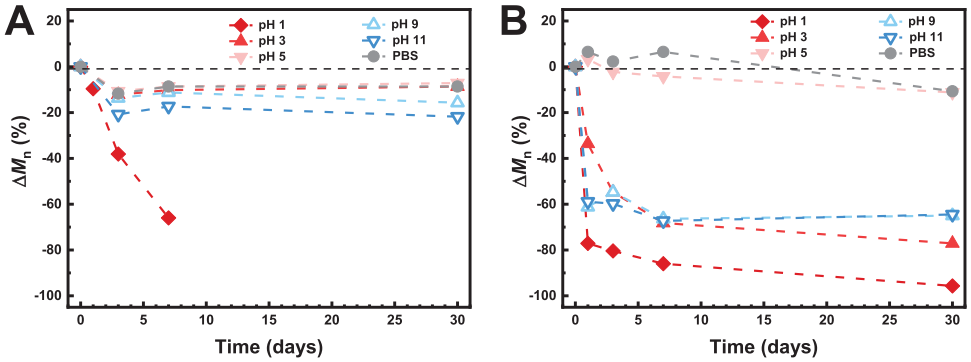

Figure 2. Evolution of M_n of A) p(D) and B) p($D_{91\%}$-$BM_{9\%}$) after hydrolytic degradation at different pH conditions and 25 °C (c = 10 mg·mL^{-1}).

backbone is at 6400 g·mol^{-1}. This is in accordance with the obtained M_n and suggests full hydrolysis of the side chains after 7 days at pH 1. Milder conditions with pH 3, 5, 7.4, 9, and 11 showed a decrease of M_n of p(D) ≈10–20% in 30 days (Figure S12, Supporting Information). SEC analysis yielded values for M_n of 18 000–15 400 g·mol^{-1} between pH 3 and 11, indicating incomplete side chain hydrolysis.

Next, we investigated the copolymer with 9% of BMDO (Figure 2B; Figures S13 and S14, Supporting Information). At pH 13 after 24 h and pH 1 after 30 d, complete degradation is observed, yielding oligomers due to degradation of the backbone, as well as products due to cleavage of DMLA side chains according to NMR and SEC. The presence of only oligomers indicates that BMDO was homogeneously incorporated along the backbone. At pH 3, 9 and 11, the molecular weight of p($D_{91\%}$–$BM_{9\%}$) decreased ≈ 60% to 70% from 21400 g·mol^{-1} to 7600–5000 g·mol^{-1} in 30 days. As this is significantly more degradation than with homopolymer p(D), this additionally confirms that the degradation of esters of side groups and in the backbone (from BMDO) occurred concurrently.

Furthermore, we assessed the degradation of p(D-BM-BP) surface-attached hydrogels (**Figure 3**A; Figure S15, Supporting Information). Here, the degradation could undergo by ester hydrolysis of i) main chain BMDO, ii) side chain DMLA, and iii) side chain BPA. For these studies, we started with an initial thickness of the coatings of ≈ 80 nm to allow for detection of significant changes. The incubation in PBS at pH 7.4 led to no degradation after 2 months, demonstrating that the coatings are stable at physiological ionic strength and pH. However, after 1 h at pH 13, the remaining thickness of all hydrogels was less than 10%

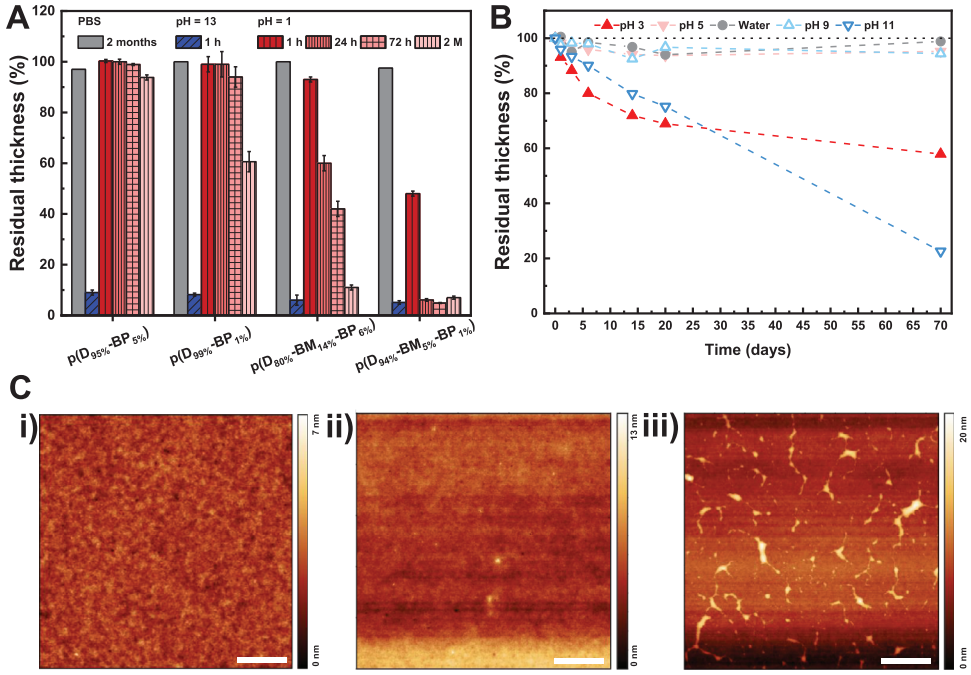

Figure 3. A) Hydrolytic degradation of surface-attached hydrogels under accelerated conditions (i.e. pH 1 and 13) at different time intervals. B) Degradation kinetics of p($D_{80\%}$-$BM_{14\%}$-$BP_{6\%}$) hydrogel at 37 °C at different pH conditions.). C) AFM images of p($D_{80\%}$-$BM_{14\%}$-$BP_{6\%}$) hydrogel coating during degradation experiments: i) initial, ii) hydrogel coating degraded to 80% of its initial thickness, and iii) hydrogel coating to less than 5% of its initial thickness. (scale bars = 1 µm).

regardless of its BMDO content. Such massive reduction in the thickness cannot be associated to the DMLA hydrolysis but necessitate the cleavage of structural components of the network, i.e. BPA and BMDO esters. The hydrolysis of BMDO and the ester bonds of BPA leads to the release of every fragment from the surface, including the crosslinks. Similar results were obtained at pH 1 but over the course of 72 h. At pH 9 and 3, the reduction of thickness was slower and stabilized to 20% and 60% while other milder pH accounted for almost no change in thickness (Figure 3A).

We additionally analyzed the hydrolysis of p(D-BP) surface-attached hydrogels. Similarly to above, the thickness reduced by 90% in pH 13 after 1 day while at pH 1 reductions in thickness of 10–40% were observed over the course of 2 months. The stability of the backbone at pH 1 is in accordance with results in solution. The higher degradability of the hydrogels with a lower content of BPA is likely attributable to their weaker mechanical stability as consequence of their low cross-linking density.

P(D-BP-BM) surface-attached hydrogels reduced their thickness by 90–40% in pH 13 and pH 1 respectively after 1 day. After 2 months at pH 1, complete degradation is observed. Low BPA content led to degradation faster due to mechanical cleavage as seen before. Moreover, as T_{cp} of p($D_{80\%}$-$BM_{14\%}$-$BP_{6\%}$) terpolymer was lower than 37 °C, it is expected that the hydrogel remained in its collapsed stated during degradation experiments, increasing its hydrophobicity and thus reducing its ability to undergo hydrolysis. Concluding, incorporation of BMDO led to significantly faster degradation due to its hydrolysis cleaving the backbone.

The surfaces before and after degradation were examined by atomic force microscopy (AFM) to investigate whether the degradation of the ultrathin surface-bound hydrogels occurs by heterogeneous detachment of polymer patches from the surface or by homogeneous degradation of the polymer chains (Figure 3C; Figure S16, Supporting Information). The initial and the partially degraded hydrogel coatings both showed a homogeneous coverage across the surface. This suggests that the degradation of the hydrogel takes place by gradual degradation along the polymer chains, ensuring similar surface properties upon degradation along the entire surface. However, when the ellipsometric thickness of the coating was below 4 nm the topographic image exhibits patches of larger height on the surface surrounded by the bare substrate. This can be attributed to residual polymers on the surface that were not detached by hydrolysis. The patches covered less than 9% of the total area, which indicates that hydrolysis has almost entirely restored the substrate. Moreover, we determined the water contact angles after 2 months of degradation of p($D_{80\%}$-$BM_{14\%}$-$BP_{6\%}$) coated silicon substrates, which showed an increase from 41° ± 2° to 71° ± 1°, demonstrating the removal of the coatings. The ability to be stable under physiological conditions but erasable under externally triggered conditions may open new avenues for these coatings in medical devices.

2.4. Cell Viability of Fibroblasts After Contact with the Coatings

Cytotoxicity can arise from positive charges within a substrate due to electrostatic interactions. It is important to note that DMLA has amide bonds, which are polybasic (e.g. Nylon 66: $K_b \approx 7$).[66] Hence, we consider it unlikely to be protonated, which is in line with the NMR spectra. Moreover, in case of positive charges in the polymer, the negatively charged albumin would be more attracted, which was not observed in the SPR studies. The effect of the coatings on the cell viability of MRC-5 fibroblasts was assessed by incubating bare and coated PMP substrates with the cells in medium at 37 °C for 24 h. No significant decrease in cell viability was observed upon direct contact with the coatings, indicating their non-cytotoxicity (Figure S18, Supporting Information).

2.5. Antifouling Properties of the Coatings at Different Temperatures

The ability of the coatings to repel proteins was investigated using SPR (**Figure 4**). For that, gold SPR sensor slides were coated with PCL, PDMS, and PP to evaluate the performance of medical polymers regarding antifouling properties, as well as with the ultrathin surface-attached hydrogels. Then, solutions of HSA (the most abundant protein in blood) and undiluted human BP were flown over bare and coated surfaces at 25 °C. The contact of the HSA and BP solutions resulted in strong fouling on the uncoated surfaces ($\Gamma_{BP,\,PMP} = 83$ ng·cm^{-2}, $\Gamma_{BP,\,PDMS} = 152$ ng·cm^{-2}, $\Gamma_{BP,\,PCL} = 226$ ng·cm^{-2}, $\Gamma_{BP,\,PP} = 170$ ng·cm^{-2} $\Gamma_{BP,\,Gold} = 324$ ng·cm^{-2}). This emphasizes the potential to improve state-of-the-art medical device surface to mitigate surface-associated complications in the body. Upon coating the gold SPR sensor slides with the ultrathin surface-attached hydrogels, non-specific fouling of HSA is reduced down to 1 ng·cm^{-2} for p($D_{99\%}$-$BP_{1\%}$), completely by p($D_{80\%}$-$BM_{14\%}$-$BP_{6\%}$) and to 6 ng·cm^{-2} for p($D_{94\%}$-$BM_{5\%}$-$BP_{1\%}$). Even when challenging the coatings with undiluted human BP, they are able to significantly decrease its non-specific adsorption to 10 ng·cm^{-2} for p($D_{99\%}$-$BP_{1\%}$), 3 ng·cm^{-2} for p($D_{80\%}$-$BM_{14\%}$-$BP_{6\%}$) and to 15 ng·cm^{-2} for p($D_{94\%}$-$BM_{5\%}$-$BP_{1\%}$). Notably, despite increasing water contact angle with lower DMLA content from $\theta \approx 33°$ for p($D_{99\%}$-$BP_{1\%}$) and p($D_{94\%}$-$BM_{5\%}$-$BP_{1\%}$) to $\theta = 41°$ for p($D_{80\%}$-$BM_{14\%}$-$BP_{6\%}$) (Table 1), there is no significant change in the antifouling properties, which is in line with previous observations.[67] Moreover, we added XPS analysis of bare and coated PMP before and after contact with blood plasma for 1 h (Figure S17, Supporting Information). The contact of bare PMP with BP resulted in strong amide and amine peaks in the N1s spectrum. The same surface coated with p($D_{99\%}$-$BP_{1\%}$) and p($D_{94\%}$-$BM_{5\%}$-$BP_{1\%}$) hydrogels displayed the typical amide bonds that occur due to the presence of the polymers. After contact with BP, no changes in C1s and N1s spectrum appeared, indicating that the coatings are antifouling toward BP. Concluding, all coatings are suitable to provide outstanding antifouling properties at room temperature at the same level and partially better than the best antifouling non-degradable polymer brushes (Table S4, Supporting Information).

Due to the different T_{cp} of the polymers, with some of the polymers having T_{cp} above bodily temperature, we assessed the antifouling properties of the coatings at 37 °C. At 37 °C, the coatings showed great repellency against HSA (below 13 ng·cm^{-2}). Considering BP, coatings with p($D_{99\%}$-$BP_{1\%}$) and p($D_{94\%}$-$BM_{5\%}$-$BP_{1\%}$) achieved a reduction in BP adsorption down to 10 ng·cm^{-2} and 32 ng·cm^{-2} respectively. However, a fouling of BP of $\Gamma_{BP} =$ 133 ng·cm^{-2}, was observed on p($D_{80\%}$-$BM_{14\%}$-$BP_{6\%}$) hydrogels,

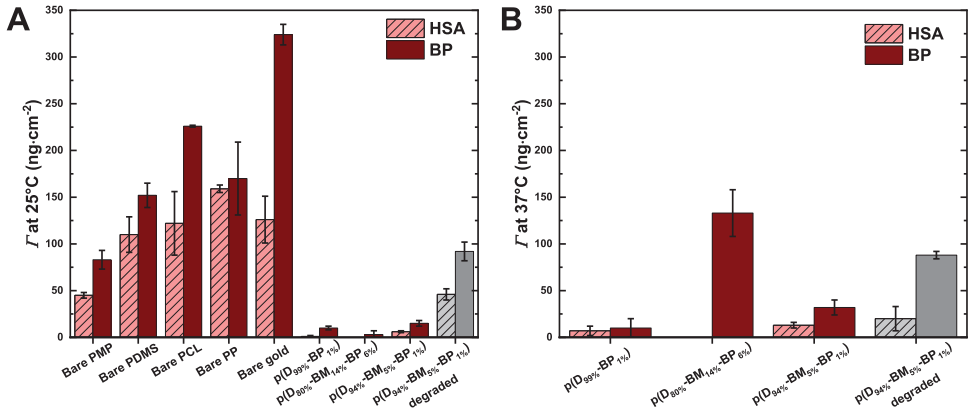

Figure 4. Fouling of HSA and undiluted human BP on bare substrates and gold SPR sensor slides coated with p($D_{99\%}$-$BP_{1\%}$), p($D_{80\%}$-$BM_{14\%}$-$BP_{6\%}$), p($DM_{94\%}$-$BM_{5\%}$-$BP_{1\%}$) and p($D_{94\%}$-$BM_{5\%}$-$BP_{1\%}$) partially degraded to a thickness of 40 nm at A) 25 °C and B) 37 °C determined with SPR ($n = 3$).

likely due to the hydrogel being in a collapsed state at 37 °C since the T_{cp} of this polymer is at 30.9 °C. The collapsed state may cause part of the polymer chains to be desolvated, thereby less swollen, impairing the steric repulsion of the brush-like interface and making it entropically less unfavorable for proteins to adsorb to the surface. Concluding, coatings of p($D_{99\%}$-$BP_{1\%}$) and p($D_{94\%}$-$BM_{5\%}$-$BP_{1\%}$) render surfaces stealth toward non-specific protein adsorption at 25 and 37 °C, while coatings with p($D_{80\%}$-$BM_{14\%}$-$BP_{6\%}$) perform best at 25 °C. Hence, for further experiments we continued with coatings of p($D_{99\%}$-$BP_{1\%}$) and p($D_{94\%}$-$BM_{5\%}$-$BP_{1\%}$). In addition to the behavior at different temperatures, we assessed the performance of p($D_{94\%}$-$BM_{5\%}$-$BP_{1\%}$) coatings after being partially degraded from a thickness of 80–40 nm. At both temperatures, the partially degraded coating exhibits significant fouling of BP. The observed increase in fouling may be attributed to one of three factors: i) generation of surface charge, ii) changes in surface energy, or iii) insufficient coating thickness. Regarding (i), we analyzed the fragments after hydrolysis by NMR and SEC. Only low molecular weight compounds could be observed that corresponded to oligo(acrylic acid), lactic acid and DML. This indicates that the degradation has to occur both in the backbone and subsequently in the side chains, thus the majority of the charged degradation products must be no longer linked to the hydrogel coating. This conclusion is supported by negligible changes in the water contact angle, measured at 34° ± 1° before degradation (thickness of 80 nm) and 30° ± 2° after partial degradation (thickness of 51 nm). Since no significant alteration in hydrophilicity was observed, surface charge accumulation or hydrophilicity changes are unlikely to be the primary cause of fouling, but rather the decrease in thickness, with the concomitant decrease in the steric repulsion and presumable loss of the brush-like structure. Moreover, the AFM analysis showed that partial degradation proceed homogenously until certain thickness, thereafter resulting in the appearance of uncoated regions which could be more rapidly fouled. Lastly, p($D_{80\%}$-$BM_{14\%}$-$BP_{6\%}$) coatings were sterilized by ethylene oxide in a standardized process. The contact of undiluted BP with the sterilized p($D_{80\%}$-$BM_{14\%}$-$BP_{6\%}$) coating led to non-specific adsorption of 27 ± 3 ng·cm^{-2}. Concluding, the sterilized coating is still suitable to prohibit protein fouling by 92%.

2.6. Prevention of Bacterial Attachment on Medical Devices

The coatings were tested for their ability to inhibit bacterial attachment with a clinical strain of MRSA, as *S. aureus* is one of the most relevant pathogens for bloodstream and wound infections.[68,69] Usually, those infections occur within the first 24 h upon contact. We contacted bare and coated PCL meshes, hernia meshes, CVCs and flat PMP membranes with MRSA for 28 h at 37 °C. Afterward, the surfaces were washed and analyzed with FESEM (**Figure 5**; Figure S19 and Table S5, Supporting Information). All bare substrates show a significant coverage of the surfaces with MRSA. PCL meshes showed the highest density of bacteria on the surface, likely due to the large surface area of the dense meshes. The coverage of the bare substrates with MRSA demonstrates the possibility for improvement of even the best state-of-the-art medical substrates. Coating the substrates with p($D_{99\%}$-$BP_{1\%}$) or p($D_{94\%}$-$BM_{5\%}$-$BP_{1\%}$) significantly reduces the coverage of the surfaces with MRSA. This is in line with the calculated low Chen Qi ratios (Table 2) and demonstrates the potential of the coatings to protect medical surfaces at the most critical time phase for bacterial infections (≈ 24 h). Moreover, we performed further exposure studies with p($D_{94\%}$-$BM_{5\%}$-$BP_{1\%}$) and p($D_{99\%}$-$BP_{1\%}$) coatings in contact with MRSA for 48 h and 96 h, demonstrating almost complete repulsion even after 96 h (Figure S20 and Table S6, Supporting Information). Hence, both coatings show strong repellency against MRSA, highlighting their potential to improve treatment outcomes for a wide spectrum of medical devices exposed to bacteria.

2.7. Protection Against Thrombus Formation on Medical Device Surfaces

To investigate the performance of the coatings in blood, we compared the fouling of blood on Hernia meshes, CVCs, and flat PMP. Hernia meshes and CVCs were taken from state-of-the-art devices used in today's clinics. PMP serves as a model for ECMOs. Bare and coated surfaces were immersed in human blood from three donors for 90 min at 37 °C. Afterward, the surfaces were rinsed and analyzed with FESEM (**Figure 6**; Figure S21,

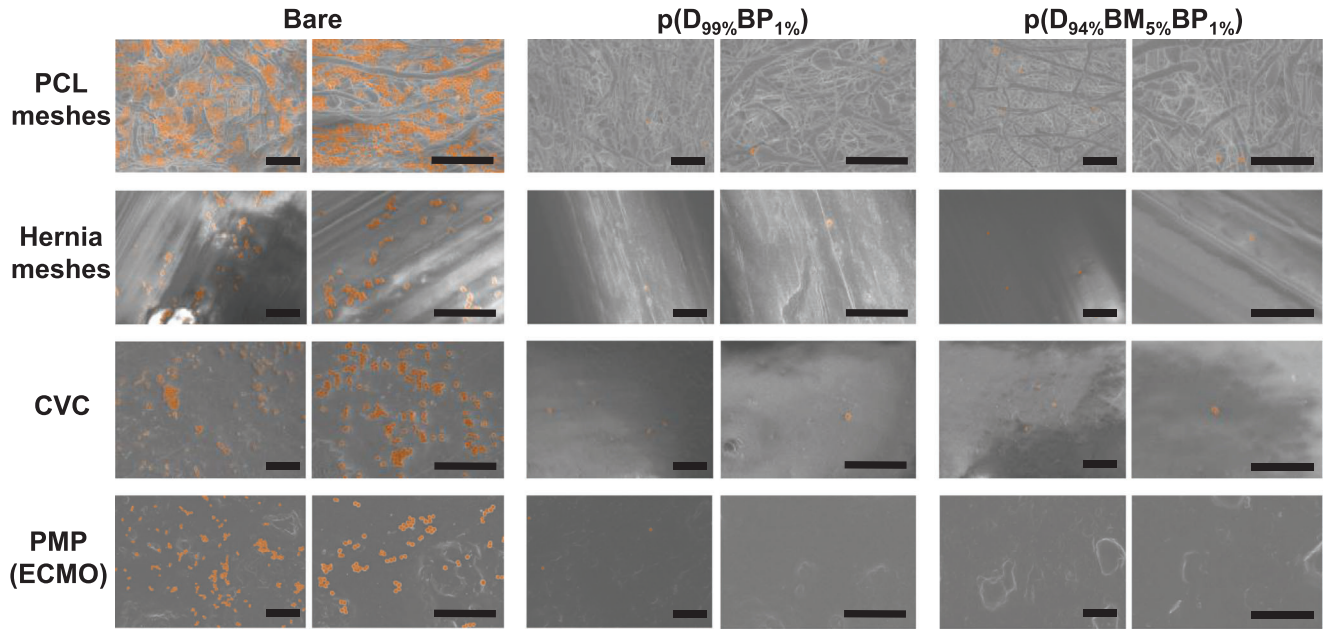

Figure 5. FESEM images of bare and coated PCL meshes, hernia meshes, CVCs, and flat PMP after contact with MRSA for 26 h at 37 °C (scale bar = 10 µm). The images were false-colored for improved visualization.

Supporting Information). Formation of protein sheaths and occupation of the surface with blood components were ubiquitous in all bare substrates, even in the most advanced state-of-the-art medical surface.[70–72] Remarkably, after coating the substrates, the surfaces exhibited a considerably lower amount of blood deposits on the surface. Hence, the coatings successfully suppressed the formation of fibrin networks on the surfaces, indicating an improved treatment outcome with these devices.

3. Conclusion

We developed antifouling green solvent-based surface-attached hydrogels with a programmable time of life, that turn a variety of different medical surfaces stealth toward complex biological fluids. In this way, they protect them against non-specific protein adsorption, colonization of MRSA, as well as the formation of thrombi on the surfaces. Their ease of application paired with partially bio-based origin and option for degradability makes them attractive as future coatings to improve the biocompatibility of a plethora of medical devices and minimize their surface-associated complications, but also could be beneficial for other scientific and industrial fields.

4. Experimental Section

Materials: Chemical reagent utilized were purchased at the highest available purity and used without further purification unless stated. Water was purified with a Millipore Milli-Q system to obtain Milli-Q water. Ethanol (EtOH, >99.8%), methanol (>99%) and anhydrous dimethylsulfoxide (DMSO, >99%) were purchased from

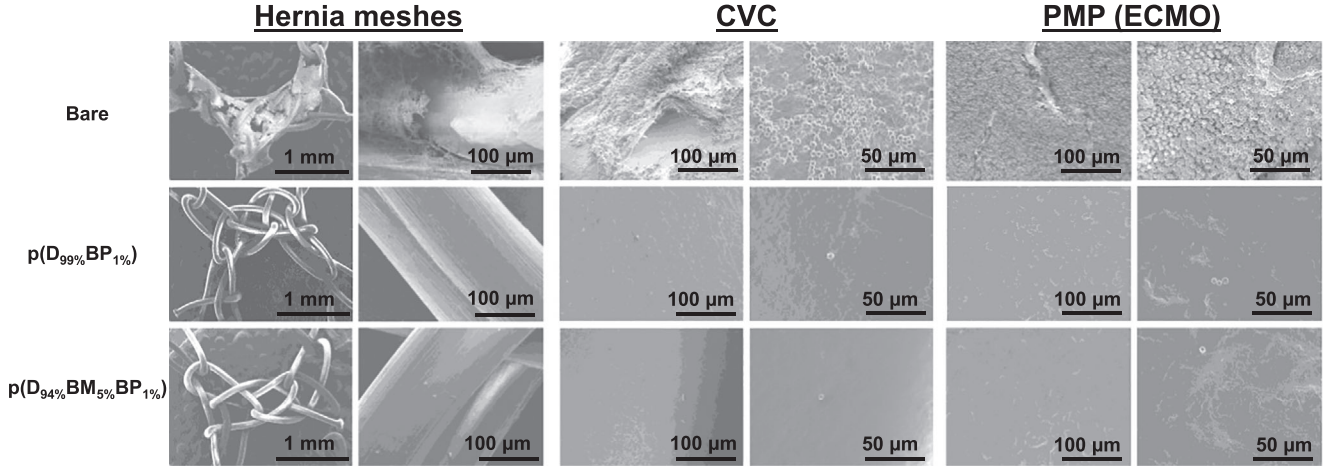

Figure 6. FESEM images of bare and coated Hernia meshes, CVCs, and flat PMP after static contact with blood from three donors for 90 min at 37 °C.

VWR International GmbH. Human serum albumin (HSA, ≥98%), citrated human blood plasma (BP), bromoacetaldehyde diethyl acetal (97%), dialysis tube benzoylated (molecular weight cut-off, MWCO, 2000), phosphate buffered saline tablets (PBS), 4-cyano-4-[(dodecylsulfanylthiocarbonyl)sulfanyl]pentanoic acid (CDSPA, 97%), anhydrous dichloromethane (DCM, >99.9%), trimethylamine (≥99%), triethylamine (TEA, ≥99.5%), 4-hydroxybenzophenone (≥98%), propylphosphonic anhydride solution (T3P, ≥50 wt. % in ethyl acetate), dibuthyl phthalate (99%), lithium aluminum hydride ($LiAlH_4$, 95%), *p*-toluenesulfonic acid (≥98.5%), sodium hydroxide (≥97%) and hydrochloric acid (37%) were obtained from Sigma Aldrich. 2,2′-Azobis(2-methylpropionitrile) (AIBN, 98%) was purchased from Sigma Aldrich and recrystallized in methanol prior to use. 2-Methyltetrahydrofuran (MeTHF, ≥99.5%) and tetrahydrofuran (THF, ≥99.0%) were purchased from Sigma Aldrich and distilled prior to use from sodium/benzophenone. CASO broth was obtained by Carl Roth. SPR gold sensor slides were purchased from Cenibra GmbH (BioNavis). Flat PMP membranes obtained by cutting polymer films (150 mm × 150 mm × 0.5 mm), which were obtained by Goodfellow Cambridge Limited. Single-lumen LifeCath central venous catheters (CVC) were kindly provided by Vygon GmbH & Co.KG. Optilene Meshes (Hernia meshes) of poly(ethylene) and poly(propylene) were purchased from B. Braun. Electrospun PCL fibers were purchased from the Institute of Textile Technology (Aachen, Germany). 1-octadecanethiol was obtained from ProChimia. *N*-octadecyltrichlorosilane (97%) was acquired from Gelest. Agnique AMD 3L (2-hydroxy-*N*,*N*-dimethyl propenamide, DML) was kindly donated by BASF SE (Ludwigshafen, Germany).

Synthesis of 1-(Dimethylamino)-1-Oxopropan-2-yl Acrylate (DMLA): A round-bottomed flask was charged with a solution of DML (20.0 mL, 1.8 mol, 1 eq.) in anhydrous MeTHF (200 mL). Then, acrylic acid (15.0 mL, 2.2 mol, 1.2 eq.), TEA (38.0 mL, 2.7 mol, 1.5 eq.), and T3P (125 mL, 2.1 mmol, 1.2 eq.) were added under Ar protection. The mixture was stirred for 24 h at room temperature. Upon completion, the solvent was eliminated under vacuum, and the residue was purified by vacuum distillation in the presence of 5 w/w % of hydroquinone. The obtained colorless oil was filtered throughout a small column of basic alumina to remove hydroquinone traces to afford DMLA (24.5 g, 80 %). ^{1}H-NMR (400 MHz, $CDCl_3$) δ 6.46 (dd, J = 17.4, 1.4 Hz, 1H), 6.18 (dd, J = 17.3, 10.4 Hz, 1H), 5.87 (dd, J = 10.4, 1.4 Hz, 1H), 5.47 (q, J = 6.7 Hz, 1H), 3.07 (s, 3H), 2.97 (s, 3H), 1.47 (d, J = 6.8 Hz, 3H).

Synthesis of 1,2-Phenylenedimethanol: The synthesis of BMDO was performed by adjusting previous literature reports.[45] In a dried round-bottomed flask, $LiAlH_4$ (11.47 g, 0.3 mol, 2 eq.) was dispersed in 200 mL of anhydrous THF under Ar cooled with an ice bath. Next, a solution of dibutyl phthalate (38 mL, 0.14 mol, 1 eq.) in 60 mL of anhydrous THF was charged to an addition funnel and added dropwise. After completion of the addition, the reaction mixture was refluxed for 16 h. Then, the mixture was cooled down to ice bath temperature and 200 mL of water containing 40 mL of H_2SO_4 was added carefully. The aqueous phase was extracted with Et_2O (3 × 100 mL) and the organic layer was washed with $NaHCO_3$ (2 × 100 mL) and water (1 × 100 mL). Finally, the organic layer was dried with $MgSO_4$ and the solvent was removed under vacuum to afford 1,2-phenylenedimethanol (16.53 g, 79%) as a white solid. The synthesis was continued without further purification. ^{1}H-NMR (400 MHz, $CDCl_3$) δ 7.30 (m, 4H), 4.63 (m, 4H), 3.67 (s, 2H)

Synthesis of 3-(Bromomethyl)-1,5-Dihydrobenzo[e][1,3]Dioxepine (BrBMDO): A mixture of 1,2-phenylenedimethanol (28.6 g, 206 mmol, 1 eq.), bromoacetaldehyde diethylacetal (30 mL, 206 mmol, 1 eq.) and *p*-toluenesulfonic acid (203.9 mg, 1.0 mmol) was heated at 120 °C under argon in a round-bottomed flask equipped with a distillation set-up. After all the calculated amount of ethanol was distilled, the temperature of the reaction mixture was raised to 140°C under reduced pressure. The crude was cooled down to room temperature and dissolved in $CHCl_3$. The organic layer was washed with a saturated solution of $NaHCO_3$ (2 × 100 mL) and water (1 × 100 mL), dried with $MgSO_4$, filtered, and the solvent was eliminated. Finally, the crude was recrystallized from cyclohexane to afford BrBMDO (41.47 g, 82%) as a pale white solid. ^{1}H-NMR (400 MHz, $CDCl_3$) δ 7.26 – 7.14 (m, 4H), 5.12 (t, J = 5.2 Hz, 1H), 4.92 (d, J = 3.8 Hz, 4H), 3.45 (d, J = 5.1 Hz, 2H).

Synthesis of 3-Methylene-1,5-Dihydrobenzo[e][1,3]Dioxepine (BMDO): A mixture of BrBMDO (20.07 g, 82.5 mmol, 1 eq.) and *t*-BuOK (13.9 g, 123.9 mmol, 1.5 eq.) in 120 mL of dried *t*-BuOH was heated to reflux under Ar for 17 h. After this, 80 mL of diethyl ether was added to the reaction mixture. The solids were removed by filtration and the organic layer was dried with $MgSO_4$ and filtered. After evaporation of the solvent, the crude product was purified by vacuum distillation to afford BMDO (9.51 g, 71%) as a white solid. ^{1}H-NMR (400 MHz, $CDCl_3$) δ 7.26–7.20 (m, 2H), 7.10–7.05 (m, 2H), 5.05 (s, 4H), 3.71 (s, 2H).

Synthesis of Benzophenone Acrylate (BPA): 4-Hydroxybenzophenone (23.7 g, 120 mmol, 1 eq.) and triethylamine (16.7 mL, 120 mmol, 1 eq.) were solubilized in anhydrous DCM (212 mL) in a three-neck-flash equipped with dropping funnel in Ar atmosphere. Acryloyl chloride (11.2 mL, 138 mmol, 1.15 eq.) was solubilized in anhydrous DCM (30 mL) and added dropwise over 30 min while cooling to 0 °C and stirring. Afterward, the reaction was allowed to proceed at room temperature for 20 h. Then, the reaction mixture was washed with brine (3 × 160 mL), sat. $NaHCO_3$ solution (1 × 160 mL) and water (1 × 160 mL). The aqueous phases were combined and extracted with DCM (2 × 160 mL). The resulting organic phases were combined, dried with $MgSO_4$ and the solvent was evaporated. The product was purified by recrystallizing it twice from ethanol.

Synthesis of p(D-BM): The copolymerization of $p(D_{90\%}\text{-}BM_{10\%})$ under the following conditions $[DMLA]_0/[BMDO]_0/[CDSPA]_0/[AIBN]_0$ = 150/50/1/0.6 is described. This procedure was generic for all the copolymerization conducted herein. A mixture of CDSPA (6.4 mg, 0.02 mmol, 1 eq.), DMLA (408.7 mg, 2.4 mmol, 150 eq.), and BMDO (128.5 mg, 0.8 mol, 50 eq.) was charged in a Schlenk tube. Then, 0.5 mL of a stock solution containing AIBN (1.6 mg, 0.01 mmol, 0.6 eq.) in anhydrous DMSO was added under Ar protection. The solution was degassed by Ar bubbling for 15 min and then immersed in a preheated oil bath at 70 °C for 15 h. After that time, the reaction was quenched by immersion in an ice bath. Next, the reaction mixture was dialyzed (MWCO 2000) against acetone, refreshing the solvent 3–4 times for 2 days. Finally, the solvent was removed to recover the synthesized polymer as a yellowish solid.

Synthesis of p(D-BM-BP): The following procedure was an example of one of the conditions used in this work. $p(D_{94\%}\text{-}BM_{5\%}\text{-}BP_{1\%})$ was synthesized by RAFT polymerization with $[DMLA]_0/[BMDO]_0/[BPA]_0/[CDSPA]_0/[AIBN]_0$ = 154/44/2/1/0.6 ratios. A mixture of CDSPA (6.3 mg, 0.02 mmol, 1 eq.), DMLA (410.0 mg, 2.4 mmol, 154 eq.), BMDO (112.1 mg, 0.7 mmol, 44 eq.), and BPA (7.6 mg, 0.03 mmol, 2 eq.) was charged in a Schlenk tube. Then, 0.5 mL of a stock solution containing AIBN (1.6 mg, 0.01 mmol, 0.6 eq.) in anhydrous DMSO was added under Ar protection. The solution was degassed by Ar bubbling for 15 min and then immersed in a preheated oil bath at 70 °C for 15 h. After that time, the reaction was quenched by immersion in an ice bath. Next, the reaction mixture was dialyzed (MWCO 2000) against acetone. The solvent was exchanged 3–4 times for 2 days. After dialysis, the polymer (yellow solid) was recovered by removing the solvent.

Determination of Conversion and Purity by Nuclear Magnetic Resonance (NMR): ^{1}H-NMR spectra were taken with a Bruker Avance III 400 spectrometer and evaluated with MestReNova (v14.2) with $CDCl_3$ or DMSO-d_6 as solvent.

Evaluation of Molecular Weights by Size Exclusion Chromatography (SEC): Moreover, molecular weight analysis was performed via SEC using an Agilent 1200 series system equipped with a precolumn (PLgel 5 µm Guard column) and a two-serial column system (2 × PLgel 5 µm MIXED-D) and with an Agilent 1100 series refractive index detector. Chromatograms were carried out in *N*,*N*-dimethyl formamide (DMF), HPLC grade, containing 0.05% (w/w) of LiBr with a flow rate of 1 mL·min^{-1} at 50°C. Samples were filtered through 0.22 µm Teflon syringe filter and 20 µL of the polymer solution was injected using a manual sample injector Rheodyne Model 7125. The calibration curves for GPC analysis were obtained with poly(methyl methacrylate) (PMMA) standards purchased from PSS Polymer Standards

Service GmbH. The molecular weights were calculated using the universal calibration principle and Mark-Houwink parameters. Toluene was used as flow rate marker.

Hydrolytic Degradation in Solution: 20 mg of p($D_{91\%}$-$BM_{9\%}$) were dissolved in 2 mL PBS (pH 7.4) or water at different pH. pH was prepared by dilution of concentrated HCl or NaOH solutions. Polymer solutions were stirred at constant speed at targeted temperature. Then, samples (0.5 mL) were withdrawn and neutralized at specific time intervals. Finally, water was removed by lyophilization, and the degradation products were then analyzed by SEC.

Hydrolytic Degradation of Surface Attached Hydrogel Coatings: Surfaces coated with hydrogels from polymers with different monomer composition were immersed in aqueous solution of different pH, which were prepared by dilution of concentrated HCl or NaOH solutions. At different time intervals, the substrates were taken out of the solutions, washed with Milli-Q water and methanol and dried under a flow of nitrogen. The hydrogel thickness was measured by ellipsometry.

Ellipsometry: The dry thicknesses were obtained with a Spectroscopic Ellipsometer M-2000X at angles of 65°, 70°, and 75°.

X-Ray Photoelectron Spectroscopy (XPS): XPS measurements were performed on an AXIS Supra+ from Kratos Analytical Ltd. An Al K alpha source with 1486.6 eV was used. Broad spectrums were acquired from 1200 to 0 eV with a step size of 1 eV and a spot size of 400 µm at 40°. Data was analyzed using the ESCApe software from Kratos and Casa XPS and all spectra were referenced to the C1s peak of hydrocarbons at 285.0 eV.

Thermodynamic Analysis: The components of the surface tension were acquired via the van Oss acid-base approach.[63,73] Details can be found in the Supporting Information.

Protein Adsorption by Surface Plasmon Resonance (SPR): Protein adsorption was determined with SPR on a MP-SPR Navi™ 210A VASA (BioNavis) with the SPR-Navi control software and SPR-Navi data viewer. The hydrogel coatings were performed either on a self-assembled organic monolayer on gold, or on spincoated poylmers. For the former, the gold SPR sensor slides were modified with a layer of 1-octadecanethiol by immersion into a solution in ethanol (1 mg·mL^{-1}) overnight, followed by rinsing with ethanol. The modification with 1-octadecanethiol allows the hydrogel coating to covalently bind to the surface. The latter includes the spincoating of a solution of e.g. PMP in toluene (10 mg·mL^{-1}) at 3000 rpm for 45 s. Then, the hydrogel was applied by spincoating the polymer solution (10 mg mL^{-1}) at 4000 rpm for 45 s. For the measurement, the surfaces were contacted with either human serum albumin (5 mg·mL^{-1} in PBS) or undiluted human BP for 60 min at 10 µg·mL^{-1}.

Atom Force Microscopy (AFM): AFM images were obtained with tapping mode on silicon substrates on a Multimode Atomic Force Microscope NanoScope V (Digital Instruments) with a nominal spring constant of 26 N·m^{-1} and a tip radius of 7 nm (OTEPSA-R3, Bruker).

Determination of Influence of the Coatings on Cell Viability: MRC-5 fibroblasts at passage 8 were seeded into 24-well plates at a density of 100 000 cells per well in DMEM supplemented with 10% FBS. The surfaces were sterilized by UV irradiation for 30 min on each side. The samples were then placed into the wells and incubated for 24 h at 37 °C. Following incubation, cell viability was assessed using the MTS assay (Promega) according to the manufacturer's instructions.

Bacterial Assay: A single colony of a clinical MRSA isolate was incubated in 10 mL CASO broth for 16 h at 100 rpm and 37 °C. The surfaces were sterilized by irradiation with UV-light for 1 h in sterile PBS. The bacterial suspension was diluted to OD_{600} of 0.22. The substrates were incubated in the diluted bacterial suspension for 26 h at 37 °C and 150 rpm, rinsed with PBS and incubated again in fresh CASO broth at 37 °C for 4 h at 150 rpm. Then, the substrates were rinsed three times with sterile PBS and fixed with glutaraldehyde (3%, 4°C, 2 h). The samples were prepared for FESEM by drying with ethanol.

Field Emission Scanning Electron Microscopy (FESEM): FESEM images were taken on carbon-sputtered samples on a FESEM S4800 from Hitachi, Japan.

Static Blood Experiments: Blood was withdrawn from three donors anonymously (approved by the Ethics Committee at the RWTH Aachen Faculty of Medicine, number: EK088/20). Blood was slightly anticoagulated with heparin (0.75 IU·mL^{-1}) to avoid instant coagulation in the syringe utilized for withdrawal. The blood was used non-pooled to allow detection of effects due to one specific donor. The samples were placed into 48 well plates and incubated with the blood for 90 min at 37 °C. Afterward, the samples were rinsed once with NaCl solution (0.9%) and three times with PBS. Then, the samples were fixed with glutaraldehyde (2%) and dried with ethanol to prepare for FESEM.

Statistical Analysis: All experiments were conducted with a sample size of at least three replicates per sample. Values are stated as the mean value with its standard deviation, which are graphically depicted as error bars.

Supporting Information

Supporting Information is available from the Wiley Online Library or from the author.

Acknowledgements

J.E. and M.P. contributed equally to this work. The authors acknowledge the support of Petra Esser who kindly provided the XPS measurements. The authors acknowledge the financial support by the German Federal Ministry of Education and Research (BMBF) with the project AntiBacCat and Heart2.0 within the "Bio4MatPro-Competence Center for Biological Transformation of Materials Science and Production Engineering" program (grant no. 031B1153A and 031B1154B), the Deutsche Forschungsgemeinschaft (DFG, German Research Foundation) via Schwerpunktprogramm "Toward an Implantable Lung" (Project number: 346972946), European Union's Horizon Europe programme IV-Lab (project number: 101115545), and IBEC which is a member of the CERCA Programme/Generalitat de Catalunya. Moreover, the authors acknowledge the research association Forschungskuratorium Textil e.V. supported via AiF ("Arbeitsgemeinschaft Industrielle Forschungsvereinigungen Otto von Guericke e.V."), research project HemoRecap (IGF-No. 22647 N) within the promotion program of "Industrielle Gemeinschaftsforschung" (IGF) of the Federal Ministry for Economic Affairs and Energy on the basic of a decision by the German Bundestag. This work was also supported through project PID2020-114098RB-I00, PID2023-149489OB-I00, and FPI grant PRE2021-100387, both founded by MICIU/AEI/10.13039/501100011033 and ESF+, and through Serra Hunter Programme of the Government of Catalonia. Moreover, the authors thank BASF SE, Ludwigshafen, Germany (Dr. O. Gronwald), for kindly supplying Agnique® AMD 3L solvent, as well as Vygon GmbH & Co.KG, Aachen, Germany, for providing CVC. O.G. had received research funding from Alexsion, Alveron, Bayer, Biotest, Boehringer Ingelheim, CSL Behring, Octapharma, Novo Nordisk, Nycomed, and Werfen.

Conflict of Interest

The authors declare no conflict of interest.

Data Availability Statement

The data that support the findings of this study are available from the corresponding author upon reasonable request.

Keywords

antifouling, biocompatibility, coating, degradability, green solvent, hydrogel, hemocompatibility

Received: February 10, 2025
Revised: April 28, 2025
Published online: May 28, 2025

[1] B. D. Ratner, A. S. Hoffman, F. J. Schoen, J. E. Lemons *Biomaterials Science: An Introduction to Materials in Medicine*, Elsevier, Amsterdam **2004**.
[2] M. Tirrell, E. Kokkoli, M. Biesalski, *Surf. Sci.* **2002**, *500*, 61.
[3] M. Thompson, C. Blaszykowski, S. Sheikh, C. Rodriguez-Emmenegger, A. De los Santos Pereira, *Biological Fluid-Surface Interactions in Detection and Medical Devices*, Royal Society of Chemistry, London **2016**.
[4] L. Vroman, *Bull. N. Y. Acad. Med.* **1988**, *64*, 352.
[5] L. Witzdam, T. White, C. Rodriguez-Emmenegger, *Macromol. Biosci.* **2024**, *24*, 2400152.
[6] S. Jeon, J. Lee, J. Andrade, P. De Gennes, *J. Colloid Interface Sci.* **1991**, *142*, 149.
[7] J. H. Lee, H. B. Lee, J. D. Andrade, *Prog. Polym. Sci.* **1995**, *20*, 1043.
[8] C. Rodriguez Emmenegger, E. Brynda, T. Riedel, Z. Sedlakova, M. Houska, A. B. Alles, *Langmuir* **2009**, *25*, 6328.
[9] Q. Ye, F. Zhou, In *Antifouling Surfaces and Materials: From Land to Marine Environment*, Springer, Berlin **2014**, pp 55-81.
[10] G. Emilsson, R. L. Schoch, L. Feuz, F. Höök, R. Y. Lim, A. B. Dahlin, *ACS Appl. Mater. Interfaces* **2015**, *7*, 7505.
[11] A. de los Santos Pereira, C. Rodriguez-Emmenegger, F. Surman, T. Riedel, A. B. Alles, E. Brynda, *RSC Adv.* **2014**, *4*, 2318.
[12] T. Riedel, Z. Riedelová-Reicheltová, P. Májek, C. Rodriguez-Emmenegger, M. Houska, J. E. Dyr, E. Brynda, *Langmuir* **2013**, *29*, 3388.
[13] Z. Riedelová, A. de los Santos Pereira, D. F. Dorado Daza, P. Májek, F. Dyčka, T. Riedel, *Macromol. Biosci.* **2024**, *24*, 2300558.
[14] C. D. Walkey, J. B. Olsen, H. Guo, A. Emili, W. C. Chan, *J. Am. Chem. Soc.* **2012**, *134*, 2139.
[15] Y. Iwasaki, K. Ishihara, N. Nakabayashi, G. Khang, J. H. Jeon, J. W. Lee, H. B. Lee, *J. Biomater. Sci., Polym. Ed.* **1998**, *9*, 801.
[16] K. Ishihara, Y. Iwasaki, S. Ebihara, Y. Shindo, N. Nakabayashi, *Colloids Surf., B* **2000**, *18*, 325.
[17] W. Feng, S. Zhu, K. Ishihara, J. L. Brash, *Langmuir* **2005**, *21*, 5980.
[18] Z. Zhang, T. Chao, S. Chen, S. Jiang, *Langmuir* **2006**, *22*, 10072.
[19] Y. Chang, S.-C. Liao, A. Higuchi, R.-C. Ruaan, C.-W. Chu, W.-Y. Chen, *Langmuir* **2008**, *24*, 5453.
[20] S. Paschke, K. Lienkamp, *ACS Appl. Polym. Mater.* **2020**, *2*, 129.
[21] T. Sakamaki, Y. Inutsuka, K. Igata, K. Higaki, N. L. Yamada, Y. Higaki, A. Takahara, *Langmuir* **2018**, *35*, 1583.
[22] H. Vaisocherova, W. Yang, Z. Zhang, Z. Cao, G. Cheng, M. Piliarik, J. Homola, S. Jiang, *Anal. Chem.* **2008**, *80*, 7894.
[23] M. Vorobii, A. de los Santos Pereira, O. Pop-Georgievski, N. Y. Kostina, C. Rodriguez-Emmenegger, V. Percec, *Polym. Chem.* **2015**, *6*, 4210.
[24] C. Rodriguez-Emmenegger, O. A. Avramenko, E. Brynda, J. Skvor, A. B. Alles, *Biosens. Bioelectron.* **2011**, *26*, 4545.
[25] F. Surman, T. Riedel, M. Bruns, N. Y. Kostina, Z. Sedláková, C. Rodriguez-Emmenegger, *Macromol. Biosci.* **2015**, *15*, 636.
[26] A. R. Kuzmyn, A. T. Nguyen, L. W. Teunissen, H. Zuilhof, J. Baggerman, *Langmuir* **2020**, *36*, 4439.
[27] C. Zhao, L. Li, J. Zheng, *Langmuir* **2010**, *26*, 17375.
[28] C. Rodriguez-Emmenegger, M. Houska, A. B. Alles, E. Brynda, *Macromol. Biosci.* **2012**, *12*, 1413.
[29] J. N. Kizhakkedathu, J. Janzen, Y. Le, R. K. Kainthan, D. E. Brooks, *Langmuir* **2009**, *25*, 3794.
[30] Y. Zou, P.-Y. J. Yeh, N. A. Rossi, D. E. Brooks, J. N. Kizhakkedathu, *Biomacromolecules* **2010**, *11*, 284.
[31] J. N. Kizhakkedathu, D. E. Brooks, *Macromolecules* **2003**, *36*, 591.
[32] H. Vaisocherová, V. Ševců, P. Adam, B. Špačková, K. Hegnerová, A. de los Santos Pereira, C. Rodriguez-Emmenegger, T. Riedel, M. Houska, E. Brynda, *Biosens. Bioelectron.* **2014**, *51*, 150.
[33] N. D. Brault, C. Gao, H. Xue, M. Piliarik, J. Homola, S. Jiang, Q. Yu, *Biosens. Bioelectron.* **2010**, *25*, 2276.
[34] J. Englert, M. Palà, L. Witzdam, F. Rayatdoost, O. Grottke, G. Lligadas, C. Rodriguez-Emmenegger, *Langmuir* **2023**, *39*, 18476.
[35] T. Riedel, A. de los Santos Pereira, J. Táborská, Z. Riedelová, O. Pop-Georgievski, P. Májek, K. Pečánková, C. Rodriguez-Emmenegger, *Macromol. Biosci.* **2022**, *22*, 2100460.
[36] M. Morbidelli, M. Romio, Y. Chandorkar, A. Gogos, C. Hirsch, B. Kolrosova, L. Trachsel, F. Lorandi, D. Badocco, P. Pastore, G. Arrigoni, C. Franchin, R. Tavano, R. Hoogenboom, E. Papini, E. M. Benetti, *Biomacromolecules* **2025**, *26*, 556.
[37] N. Bentley, F. D. Scherag, T. Brandstetter, J. Rühe, *Adv. Mater. Interfaces* **2022**, *9*, 2102359.
[38] O. Prucker, T. Brandstetter, J. Rühe, *Biointerphases* **2018**, *13*, 010801.
[39] R. Toomey, D. Freidank, J. Rühe, *Macromolecules* **2004**, *37*, 882.
[40] L. Witzdam, Y. L. Meurer, M. Garay-Sarmiento, M. Vorobii, D. Söder, J. Quandt, T. Haraszti, C. Rodriguez-Emmenegger, *Macromol. Biosci.* **2022**, *22*, 2200025.
[41] L. Witzdam, M. Garay-Sarmiento, M. Gagliardi, Y. L. Meurer, Y. Rutsch, J. Englert, S. Philipsen, A. Janem, R. Alsheghri, F. Jakob, *Macromol. Biosci.* **2023**, *24*, 2300434.
[42] M. Palà, H. El Khannaji, M. Garay-Sarmiento, J. C. Ronda, V. Cádiz, M. Galià, V. Percec, C. Rodriguez-Emmenegger, G. Lligadas, *Green Chem.* **2022**, *24*, 8314.
[43] N. Migliore, A. Guzik, M. C. Stuart, M. Palà, A. Moreno, G. Lligadas, P. Raffa, *ACS Sustain. Chem. Eng.* **2022**, *10*, 14806.
[44] N. Bensabeh, A. Moreno, A. Roig, M. Rahimzadeh, K. Rahimi, J. C. Ronda, V. Cádiz, M. Galià, V. Percec, C. Rodriguez-Emmenegger, *ACS Sustain. Chem. Eng.* **2019**, *8*, 1276.
[45] H. Wickel, S. Agarwal, *Macromolecules* **2003**, *36*, 6152.
[46] J. Englert, L. Witzdam, D. Söder, M. Garay-Sarmiento, A. Joseph, A. M. Wagner, C. Rodriguez-Emmenegger, *Macromol. Chem. Phys.* **2023**, *224*, 2300306.
[47] A. Bossion, C. Zhu, L. Guerassimoff, J. Mougin, J. Nicolas, *Nat. Commun.* **2022**, *13*, 2873.
[48] J.-B. Lena, A. M. Van Herk, *Ind. Eng. Chem. Res.* **2019**, *58*, 20923.
[49] H. Wickel, S. Agarwal, A. Greiner, *Macromolecules* **2003**, *36*, 2397.
[50] R. Barbey, L. Lavanant, D. Paripovic, N. Schuwer, C. Sugnaux, S. Tugulu, H.-A. Klok, *Chem. Rev.* **2009**, *109*, 5437.
[51] O. Prucker, C. A. Naumann, J. Rühe, W. Knoll, C. W. Frank, *J. Am. Chem. Soc.* **1999**, *121*, 8766.
[52] H. Murata, B.-J. Chang, O. Prucker, M. Dahm, J. Rühe, *Surf. Sci.* **2004**, *570*, 111.
[53] C. Pandiyarajan, O. Prucker, B. Zieger, J. Rühe, *Macromol. Biosci.* **2013**, *13*, 873.
[54] K. Li, C. K. Pandiyarajan, O. Prucker, J. Rühe, *Macromol. Chem. Phys.* **2016**, *217*, 526.
[55] J. K. Meinzer, M. Henze, C. K. Pandiyarajan, O. Prucker, W. Bothe, F. Beyersdorf, J. Rühe, *ASAIO J.* **2022**, *68*, 56.
[56] M. Nimni, L. Wise, D. Trantolo, D. Altobelli, M. Yaszemski *Encyclopedic Handbook of Biomaterials and Bioengineering: Part A: Materials*, Taylor & Francis, New York, NY, USA **1995**.
[57] P. W. Beines, I. Klosterkamp, B. Menges, U. Jonas, W. Knoll, *Langmuir* **2007**, *23*, 2231.
[58] A. Mateescu, Y. Wang, J. Dostalek, U. Jonas, *Membranes* **2012**, *2*, 40.
[59] S. K. Christensen, M. C. Chiappelli, R. C. Hayward, *Macromolecules* **2012**, *45*, 5237.
[60] T. He, D. Jańczewski, S. Jana, A. Parthiban, S. Guo, X. Zhu, S. S. C. Lee, F. J. Parra-Velandia, S. L. M. Teo, G. J. Vancso, *J. Polym. Sci. Part A: Polym. Chem.* **2016**, *54*, 275.
[61] S. Guo, X. Zhu, M. Li, L. Shi, J. L. T. Ong, D. Jańczewski, K. G. Neoh, *ACS Appl. Mater. Interfaces* **2016**, *8*, 30552.
[62] G. B. Sigal, C. Bamdad, A. Barberis, J. Strominger, G. M. Whitesides, *Anal. Chem.* **1996**, *68*, 490.
[63] C. J. Van Oss, M. K. Chaudhury, R. J. Good, *Chem. Rev.* **1988**, *88*, 927.
[64] C. Liu, Q. Zhao, *Biofouling* **2011**, *27*, 275.
[65] C. Liu, Q. Zhao, *Langmuir* **2011**, *27*, 9512.

[66] X. Huang, B. Shi, B. Li, L. Li, X. Zhang, S. Zhao, *Polym. Test.* **2006**, *25*, 970.
[67] C. Rodriguez-Emmenegger, E. Brynda, T. Riedel, M. Houska, V. Šubr, A. B. Alles, E. Hasan, J. E. Gautrot, W. T. Huck, *Macromol. Rapid Commun.* **2011**, *32*, 952.
[68] C. K. Naber, *Clin. Infect. Dis.* **2009**, *48*, S231.
[69] K. Kirketerp-Møller, P. Ø. Jensen, M. Fazli, K. G. Madsen, J. Pedersen, C. Moser, T. Tolker-Nielsen, N. Høiby, M. Givskov, T. Bjarnsholt, *J. Clin. Microbiol.* **2008**, *46*, 2717.
[70] C. Harter, T. Ostendorf, A. Bach, G. Egerer, H. Goldschmidt, A. Ho, *Support. Care Cancer* **2003**, *11*, 790.
[71] J. Bellon, M. Rodriguez, N. García-Honduvilla, V. Gómez-Gil, G. Pascual, J. Buján, *J. Biomed. Mater. Res., Part B* **2009**, *89*, 448.
[72] E. Khoshbin, A. E. Dux, H. Killer, A. W. Sosnowski, R. K. Firmin, G. J. Peek, *Perfusion* **2007**, *22*, 15.
[73] C. J. van Oss, R. Good, R. Busscher, *J. Dispers. Sci. Technol.* **1990**, *11*, 75.